TRANSACTIONS OF THE INSTITUTE OF AVIATION eISSN 2300-5408
No. 1(238), pp. 35-53, Warsaw 2015

EXPERIMENTAL MEASUREMENTS AND SIMULATION CALCULATIONS OF LOADS IN CONTROL SYSTEM OF HELICOPTER ROTOR

JAROSŁAW STANISŁAWSKI

New Technology Center, Aircraft Design Department, Institute of Aviation, al. Krakowska 110/114, 02-256 Warsaw, Poland, stanjar@ilot.edu.pl

Abstract

Paper presents measured data of ILX-27 helicopter test in hover condition compared to simulation calculations concerning loads of a rotor control system. Used computing program for rotor loads calculation comprises a model of rotor blade treated as a elastic axis with a set of lumped masses. The results of simulation calculations also include predicted level of rotor control system loads for some other than hover states of flight.

Keywords: helicopter, blade, control system loads.

INTRODUCTION

Recently a rapid progress has been noticed in unmanned helicopter technology. Unmanned aerial vehicles (UAV) comprise rotorcrafts with take-off mass ranging from ultralight models to full-scale helicopters like MQ-8B Fire Scout (mass 1,430 kg) or K-Max Kaman UAT − Unmanned Aerial Truck (mass 5,440 kg). Also in Poland started a program of developing the large unmanned helicopter ILX-27 of similar class with the take-off mass over 1,000 kg. Designing, building and testing of ILX-27 helicopter was the task of scientific-research consortium including the Institute of Aviation (Instytut Lotnictwa), the Air Force Institute of Technology (Instytut Techniczny Wojsk Lotniczych) and Military Aviation Works No. 1 (Wojskowe Zakłady Lotnicze Nr 1).

The helicopter is built in a classic configuration with three bladed main rotor and five-bladed tail rotor (Fig. 1). Some new solutions are applied to the helicopter design [1] comprising strength structure, rotor blades, control and communication system with operation command station. The tail boom integrated with fin and shroud for tail rotor is built as a carbon fiber composite structure. The new airfoils of ILH family developed in the Institute of Aviation are applied for composite blades of the main rotor. Developing the stability augmentation system in connection with hydraulic system controlling the main rotor blade pitch, tail rotor blade pitch and engine throttle position enable flight of the unmanned helicopter. The key elements of the rotor blades control system are hydraulic actuators which provide proper linear and angular displacements of the swashplate. The simultaneous move of rods of three actuators

in the same direction realizes vertical motion of the swashplate changing the collective pitch of rotor blades. The differential displacements of actuators cause rolling or pitching the plane of the swashplate which creates the cyclic pitch of rotor blades.

After ground tests confirming the correct work of the helicopter control system the flight tests in hover were performed (Fig. 2). The hover tests include directional maneuvers, displacements at slow speed and flights in condition of hot air temperature.

Fig. 1. ILX-27 helicopter prepared for tests [J. Stanisławski, 2014]

Fig. 2. ILX-27 unmanned helicopter in hover [J. Stanisławski, 2014]

MEASUREMENTS AND SIMULATIONS

To evaluate the real level of loads generated in the rotor control system the strain gauges were attached to push rods mounted below the non-rotating part of the swashplate (Fig. 3). Basing on measurements of displacements of actuators rods the motion of the swashplate controlling the collective and cyclic pitch of rotor blade was defined. The rotation speed of the main gear input shaft and its torque were measured (Fig. 4) to get information on power required to drive the rotor. Taking into account the measured parameters the simulation calculations of rotor loads and element of rotor control system loads were executed.

The results of calculations were compared with records of flight test. Further predicting calculations were performed for other states of flight envelope. For calculation was used the modified version of in-house program code [2], [3] including geometry data for location of three push rods attached below the swashplate and realizing the mixed control of collective cyclic blade pitch. The simulation program applies the model of deformable blade consisting of the lumped mass set distributed along the elastic axis which represents blade bending and torsion stiffness (Fig. 5).

Fig. 3. Strain gauges attached to push rods below swashplate [J. Stanisławski, 2014]

Fig. 4. Localization of torque meter with circular aerial on input shaft of main gear [J. Stanisławski, 2014]

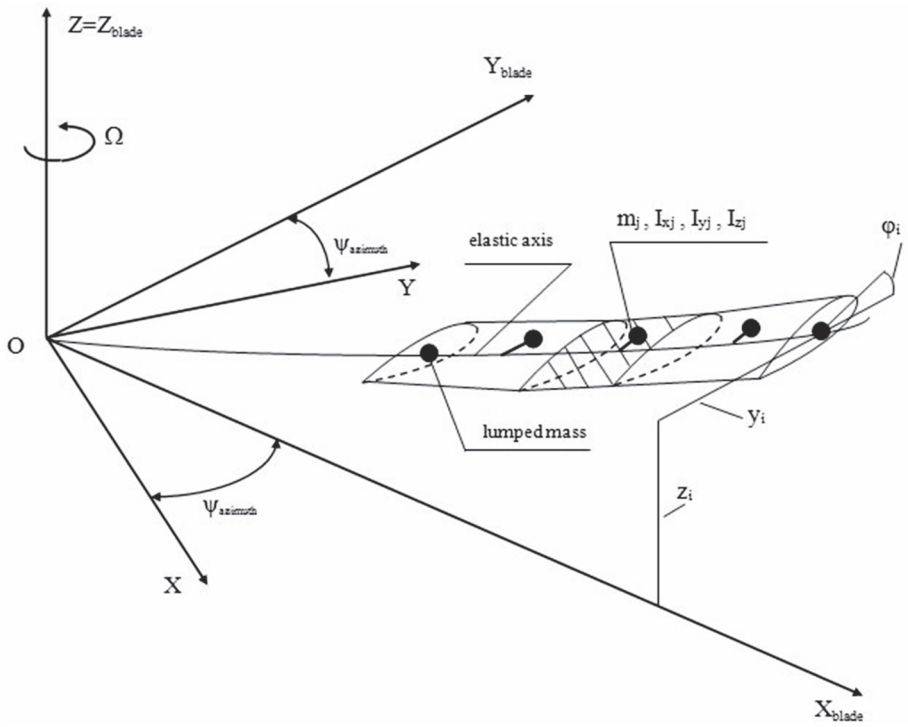

Fig. 5. Physical model of rotor blade [J. Stanisławski, 2014]

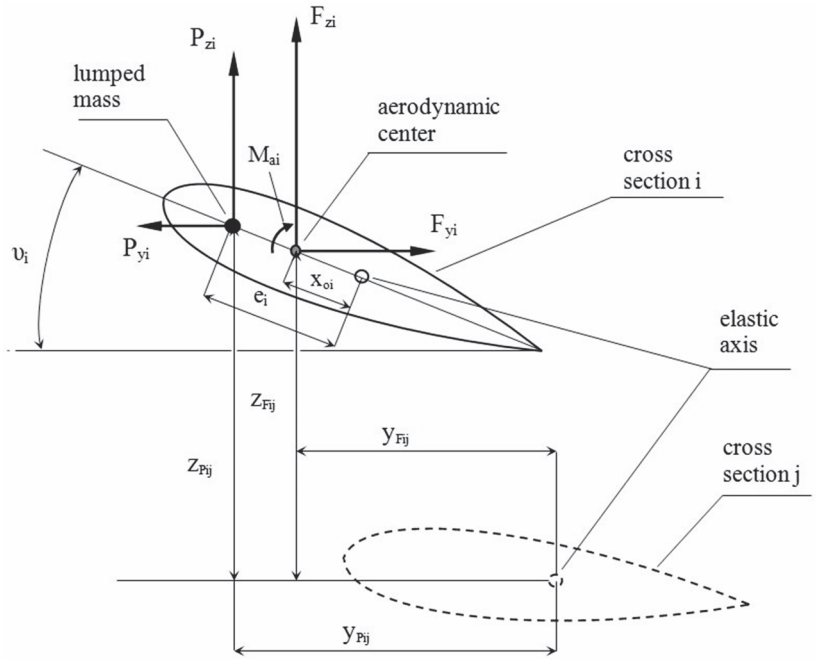

Fig. 6. Scheme of components of torsion moment in cross-section of rotor blade [J. Stanisławski, 2014]

Motion equations of deformable blade are solved using Galerkin's method taking into account eigen modes of blade vibration: bending in-plane, bending out-of-plane and torsion. The level of loads at the rotor control system largely depends on torsion moments acting on the rotor blades. For elastic blade the torsion moment in *j* cross-section depends on the relative displacements of blade outer cross-sections and local distribution of aerodynamic and inertial loads at blade segments (Fig. 6). The local torsion moment in *j* cross-section of elastic axis due to aerodynamic and inertial loads acting in *i* section is defined as follows:

$$M_{xj} = \left(P_{zi} + P_{xi} \cdot \Delta\alpha_{ij}\right) \cdot y_{Pij} - \left(P_{yi} + P_{xi} \cdot \Delta\gamma_{ij}\right) \cdot z_{Pij} + F_{zi} \cdot y_{Fij} + F_{yi} \cdot z_{Fij} + M_{ai} + M_{Ii} \tag{1}$$

where

P_{zi}, P_{yi} – inertial forces of *i* blade segment out-of rotation plane and in-plane respectively,

$P_{xi} \cdot \Delta\alpha_{ij}$, $P_{xi} \cdot \Delta\gamma_{ij}$ – components of centrifugal force due to differences of bending deflection angles between *i* and *j* cross-sections of elastic axis out-of-plane and in-plane,

F_{zi}, F_{yi} – aerodynamic forces of *i* blade segment – lift and drag,

y_{Pij}, z_{Pij} – relative displacement of *i* and *j* lumped mass measured in-plane and out-of-plane,

y_{Fij}, z_{Fij} – relative displacement of aerodynamic center at *i* and *j* section for in-plane and out-of-plane respectively,

M_{ai} – aerodynamic moment of *i* blade segment,

M_{Ii} – torsion moment of inertial forces of *i* blade segment:

$$M_{Ii} = -I_{xi} \cdot \left(\ddot{\Phi}_i + \Omega^2 \cdot \Phi_i\right) \tag{2}$$

where

I_{xi} – mass inertial moment of *i* blade segment,

Ω – rotational speed of main rotor,

$\ddot{\Phi}_i$ – angular acceleration of pitching the *i* blade segment,

Φ_i – pitch angle of *i* blade segment.

The simulations were performed for the case of an isolated rotor in condition out of ground effect. The input data for calculation were based on flight test registration. In Table 1 are collected the measured parameters taken into account for the calculation.

Table 1. Measured data for calculation of rotor control loads in hover [J. Stanisławski, 2014]

Parameter	Value
Main rotor rotation speed, Ω	46.81 rd/s
Blade collective pitch at root, φ_o	20.304°
Swashplate deflection (rolling) cyclic stick to azimuth 270°, φ_x	-0.601°
Swashplate deflection (pitching) cyclic stick to azimuth 0°, φ_y	0.875°
Torque on input shaft of main gear	637.4 Nm
Main rotor shaft power	133.07 kW
Force acting on the left push rod below swashplate, F_{LSW}	-307.4 N
Force acting on the right push rod below swashplate, F_{RSW}	-597.5 N
Force acting on the middle push rod below swashplate, F_{MSW}	-187.8 N

Additional data: helicopter take off mass 1,047 kg, outer air temperature 28°C and pressure 1,004.5 hPa.

The comparison of calculation results and flight test registrations comprises the input torque of the main gear (Fig. 10÷Fig. 12) and forces acting on push rods attached to lower non-rotating part of the swashplate (Fig. 7÷Fig. 9). The left and right push rods take part in realization of blade collective pitch, while their differential displacements cause the swashplate roll to the left or right side and following it rolling of the rotor disk due of blade cyclic pitch. The middle push rod together with left and right ones takes part in blade collective pitch. An individual motion of the middle push rod generates the swashplate pitching and then blade cyclic pitch (pull-up or push-over stick). The results of calculation are presented in form of time run plots and are collected in Table 2.

Table 2. Calculated results for rotor in hover [J. Stanisławski, 2014]

Parameter	Value
Main rotor thrust	10,260 N
Blade collective pitch at root, φ_o	20.684°
Torque on input shaft of main gear	557.5 Nm
Main rotor shaft power	116.39 kW
Force acting on the left push rod below swashplate, F_{LSW}	-302.3 N
Force acting on the right push rod below swashplate, F_{RSW}	-474.9 N
Force acting on the middle push rod below swashplate, F_{MSW}	-98.6 N

Additional information: the rotor speed and swashplate the same as given in Table 1.

The solution for hover condition concerning the forces acting on left, right and middle pushrods below the swashplate are shown in Fig. 7a÷c respectively. The calculations were conducted for quasi-static conditions without the change of the swashplate position and for steady rotor speed during simulation. The computing process was performed for twelve revolutions of the rotor which corresponds to real time period of 1.6 second. After vanishing of the initial conditions in the period of about six rotor revolutions the stable solution with limited oscillations due to swashplate deflections was obtained.

The fragments of push rod forces registration in hover test are presented in Fig. 8a÷c. The comparison of measurement data and the results of calculation of forces acting on the push rods attached below swashplate are inserted in Fig. 9a÷c.

At the given deflections of swashplate, corresponding to slightly pulled up and left side position of cyclic stick, the most loaded is the right push rod and the least loaded is the middle one. The best compatibility can be observed for measured and calculated loads acting on the left push rod (Fig. 9b). additional comparison of calculated (Fig. 10) and measurement data (Fig. 11) concerning the torsion moment on input shaft of main gear and rotor power required in hover condition are presented in Fig. 12. Obtained in calculation the lower level of shaft torsion moment related to measured torque can indicate too small value of drag coefficient of the rotor blade airfoil in block input data of a computer program. It should be noticed that in other states of flight the loads of the rotor control system can reach a much greater level than in hover condition. The results of simulation calculations for push rods below swashplate in flight at high speed (v = 180 km/h) and in pull-up condition are shown in Fig. 13÷Fig. 16.

In flight at high speed the forces acting on push rods increase even three times compared to hover level with an evident growth of oscillations. The enhanced increase of the mean level and amplitude of loads of elements of control system can be observed in pull-up and flare maneuver.

The sharp growth of control system loads oscillation is directly related to changes of airflow conditions of rotor blade sections and related to the distribution of torsion deflection and moment on the rotor disk due to azimuth and radial position of the blade section (Fig. 17÷Fig. 22). The torsion deflection of the rotor blade at tip section reaches -1.9° at high speed (Fig. 17) increasing to -3.65° twist in flare maneuver (Fig. 19). The higher torsion moments generated on the blade are observed in a flare maneuver (Fig. 20) compared to level flight conditions (Fig. 18). The large difference of blade torsion moments can be explained as the results of occurrence at the blade tip the airflow separation zone, whose border is shown as bold line in Fig. 22. In level flight condition (Fig. 21) there is no separation zone at blade tip region.

CONCLUSIONS

The measurement results and computer simulations for unmanned helicopter in hover condition concerning the loads of the rotor control system were compared. Similar levels of forces acting on push rods attached below the swashplate were obtained. The calculations predicting the loads of the rotor control system were performed for other than hover states of the helicopter flight. The developed computing program can be used to define the load level of helicopter rotor control system and to select the proper actuators allowing to control the unmanned helicopter.

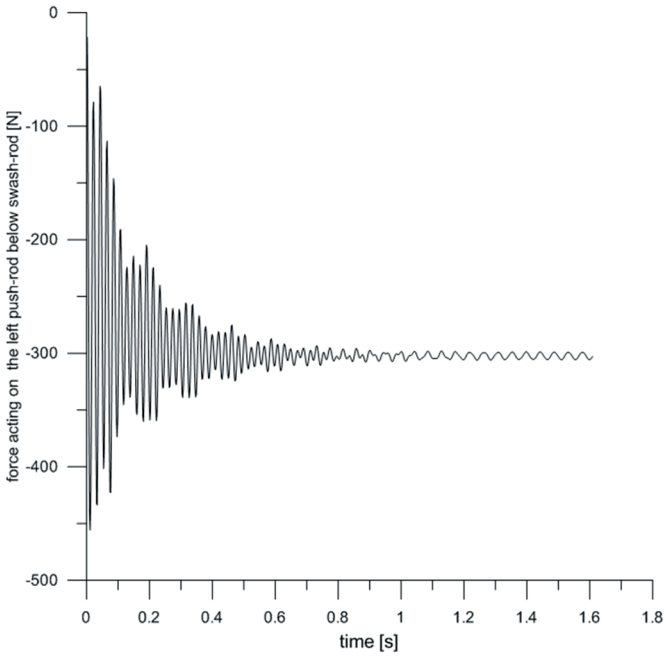

Fig. 7a. Time run of simulated solution of force acting on **the left** push rod situated below swashplate (blade collective pitch and rolling deflection of swashplate), ILX-27 helicopter, mass 1,047 kg, hover [J. Stanisławski, 2014]

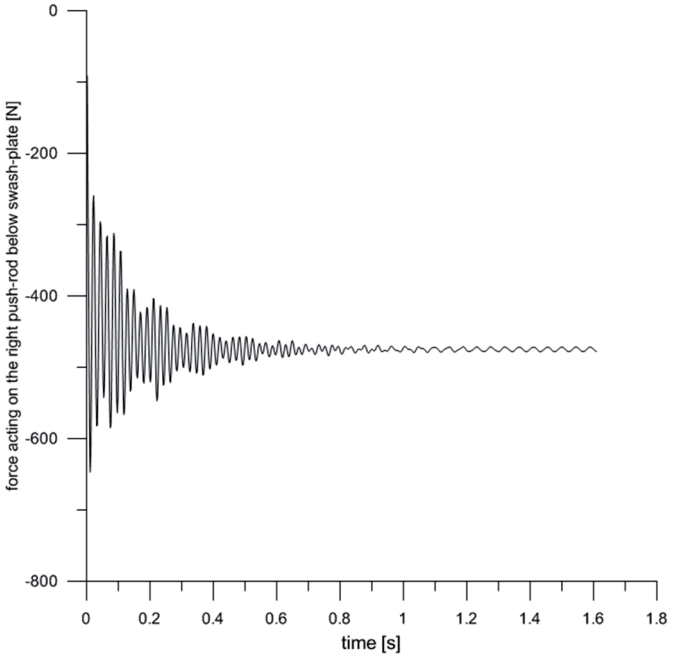

Fig. 7b. Time run of simulated solution of force acting on **the right** push rod situated below swashplate (blade collective pitch and rolling deflection of swashplate), ILX-27 helicopter, mass 1,047 kg, hover [J. Stanisławski, 2014]

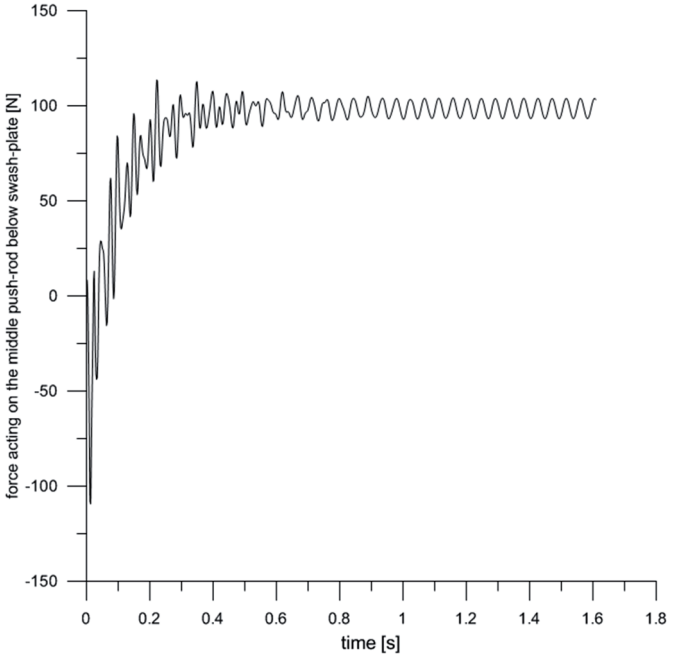

Fig. 7c. Time run of simulated solution of force acting on **the middle** push rod situated below swashplate (blade collective pitch and pitching deflection of swashplate), ILX-27 helicopter, mass 1,047 kg, hover [J. Stanisławski, 2014]

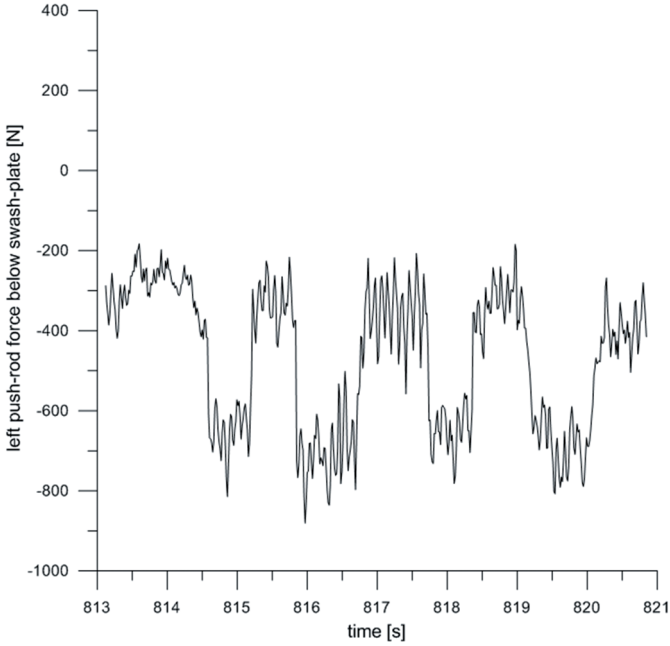

Fig. 8a. Fragment of measurement of left push rod force below swashplate, (collective pitch and rolling deflection of swashplate), ILX-27 helicopter, hover [J. Stanisławski, 2014]

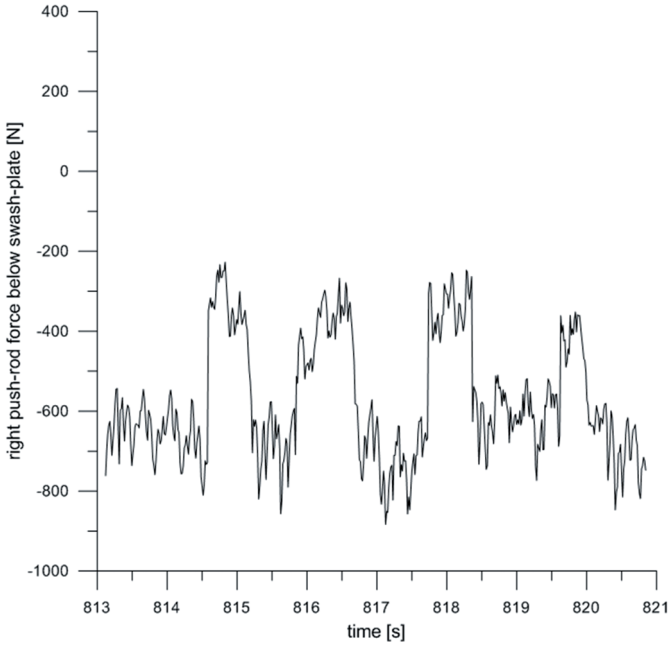

Fig. 8b. Fragment of measurement of right push-rod force below swashplate, (collective pitch and rolling deflection of swashplate), ILX-27 helicopter, hover [J. Stanisławski, 2014]

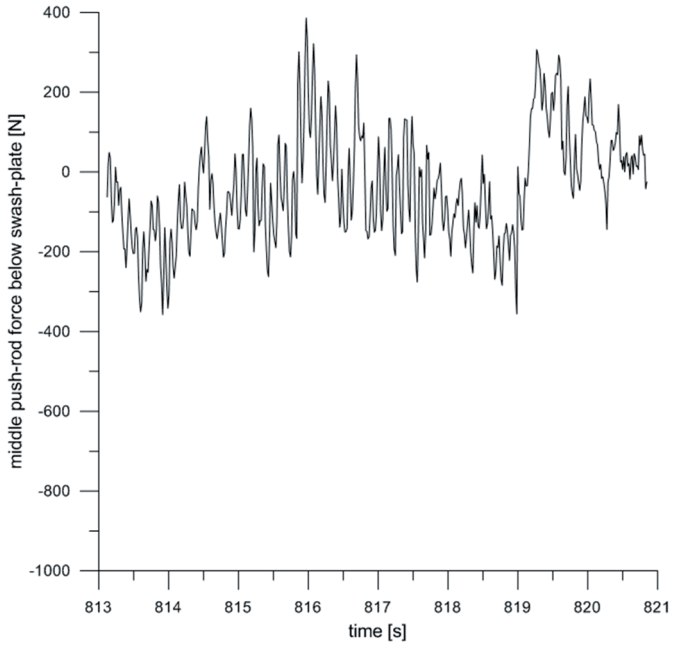

Fig. 8c. Fragment of measurement of middle push rod force below swashplate, (collective pitch and pitching deflection of swashplate), ILX-27 helicopter, hover [J. Stanisławski, 2014]

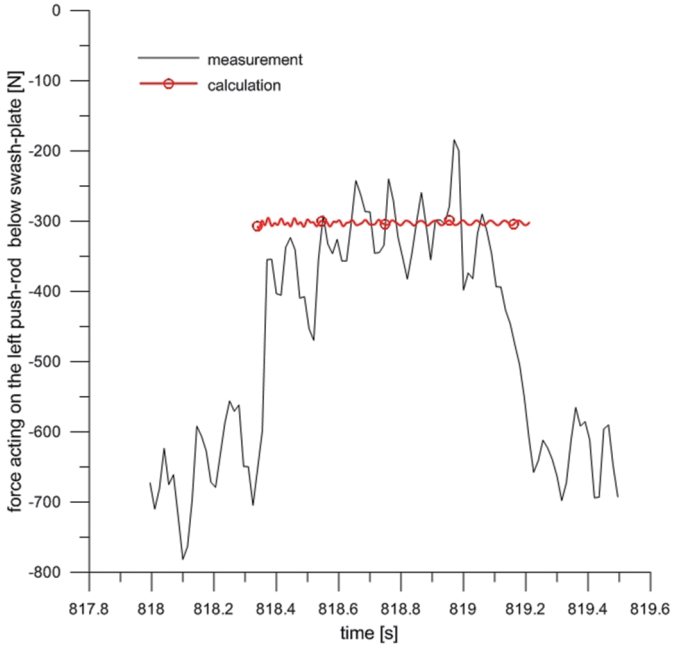

Fig. 9a. Comparison the fragment of measurement data and results of calculation for quasi static condition of force acting on the **left** push rod located below swashplate (blade collective pitch and rolling deflection of swashplate), ILX-27 helicopter, mass 1,047 kg, hover [J. Stanisławski, 2014]

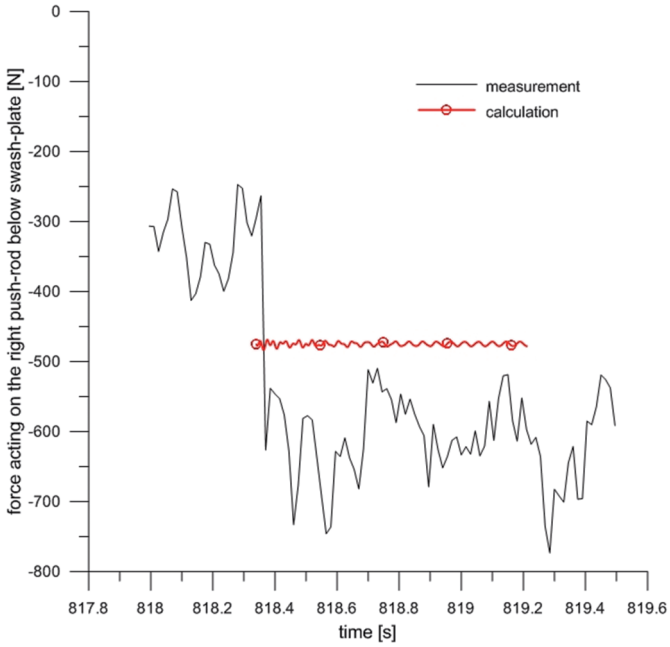

Fig. 9b. Comparison the fragment of measurement data and results of calculation for quasi static condition of force acting on the **right** push rod located below swashplate (blade collective pitch and rolling deflection of swashplate), ILX-27 helicopter, mass 1,047 kg, hover [J. Stanisławski, 2014]

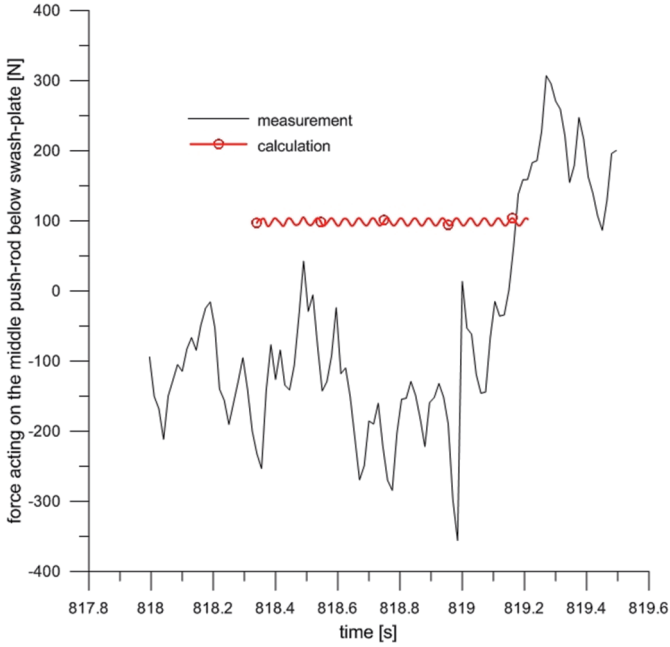

Fig. 9c. Comparison the fragment of measurement data and results of calculation for quasi static condition of force acting on the **middle** push rod located below swashplate (blade collective pitch and pitching deflection of swashplate), ILX-27 helicopter, mass 1,047 kg, hover [J. Stanisławski, 2014]

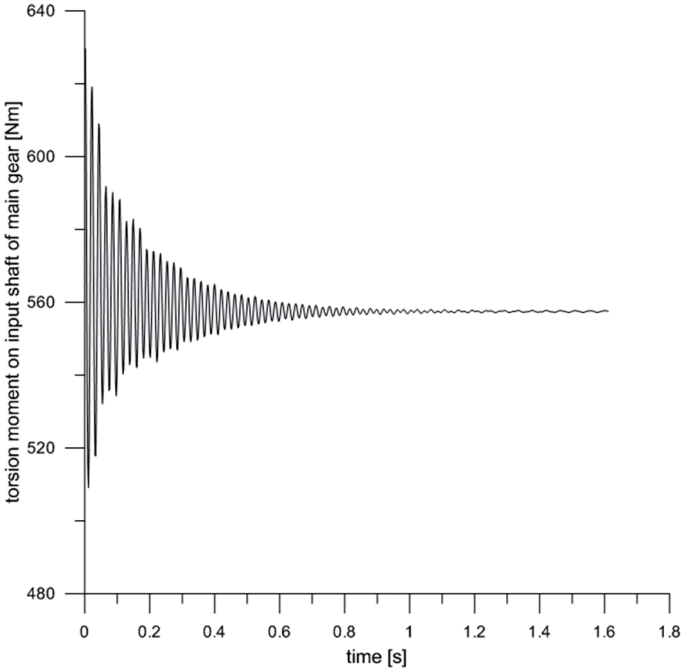

Fig. 10a.Time run of calculated torsion moment on input shaft of main gear, ILX-27 helicopter, mass 1,047 kg, hover, main gear transmission ratio i_{gear} = 4.46 [J. Stanisławski, 2014]

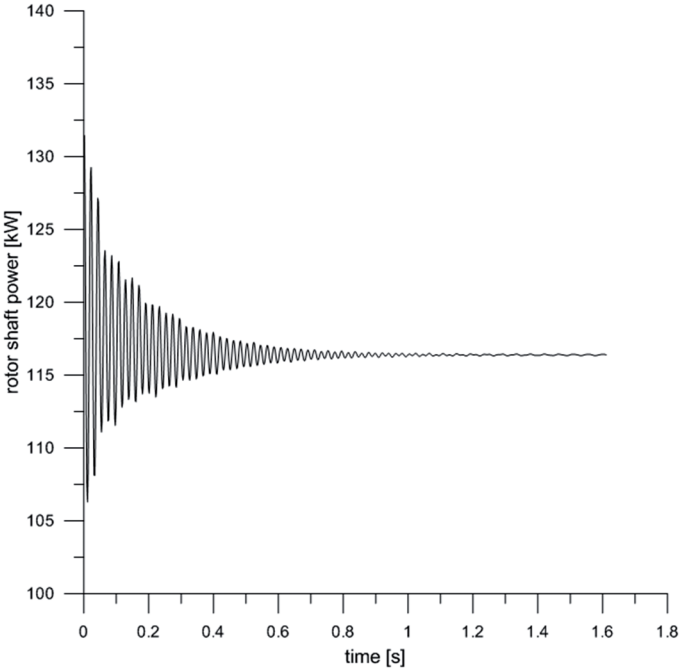

Fig. 10b. Calculation of rotor shaft power required in hover flight condition, ILX-27 helicopter, mass 1,047 kg [J. Stanisławski, 2014]

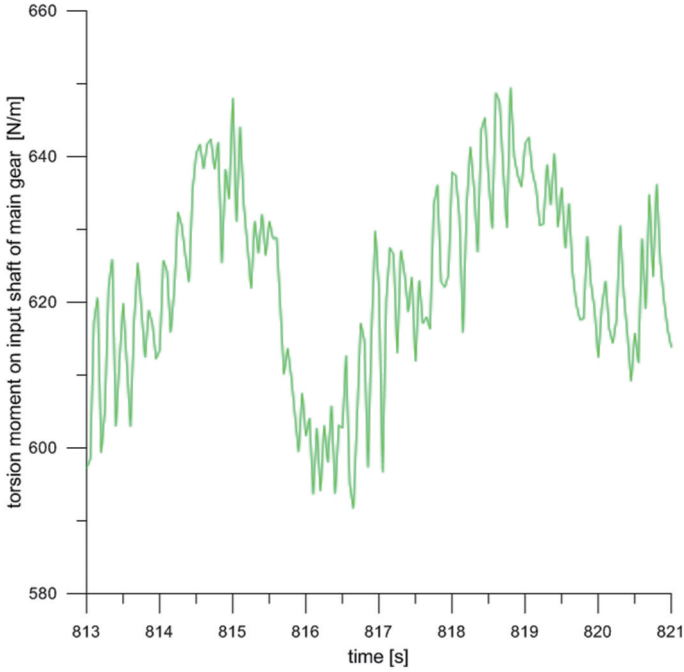

Fig. 11. Fragment of record of torsion moment on input shaft of main gear ILX-27 helicopter, mass 1,047 kg, hover [J. Stanisławski, 2014]

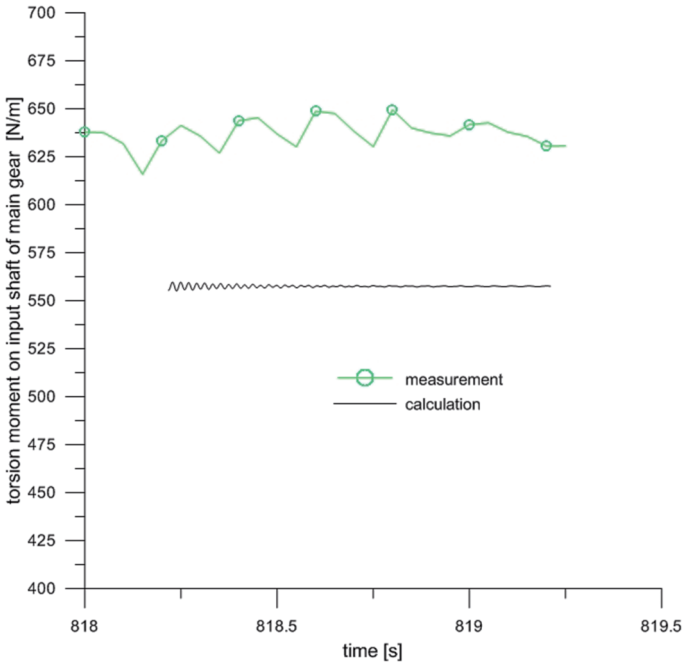

Fig. 12. Comparison of the fragment of measurement data and calculated results of torsion moment acting on input shaft of main gear ILX-27 helicopter, mass 1,047 kg, hover [J. Stanisławski, 2014]

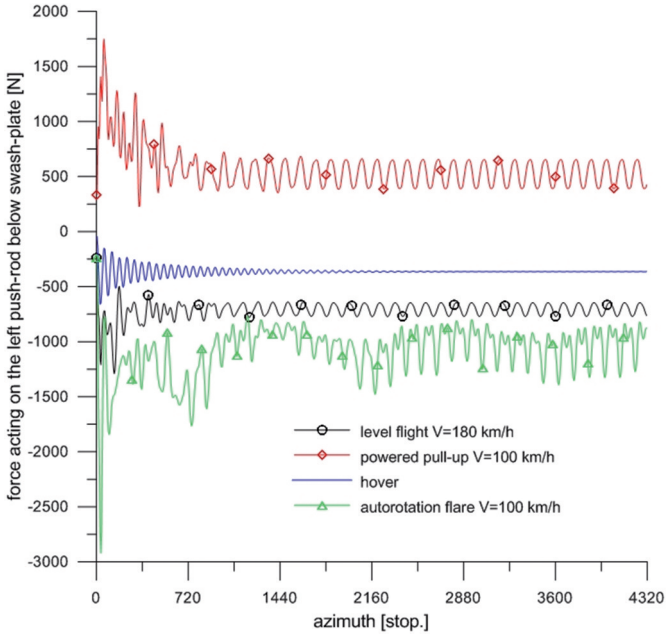

Fig. 13. Comparison of calculated loads of element of rotor control system − force acting on the left push rod below swashplate in certain states of flight ILX-27 helicopter, mass 1,100 kg [J. Stanisławski, 2014]

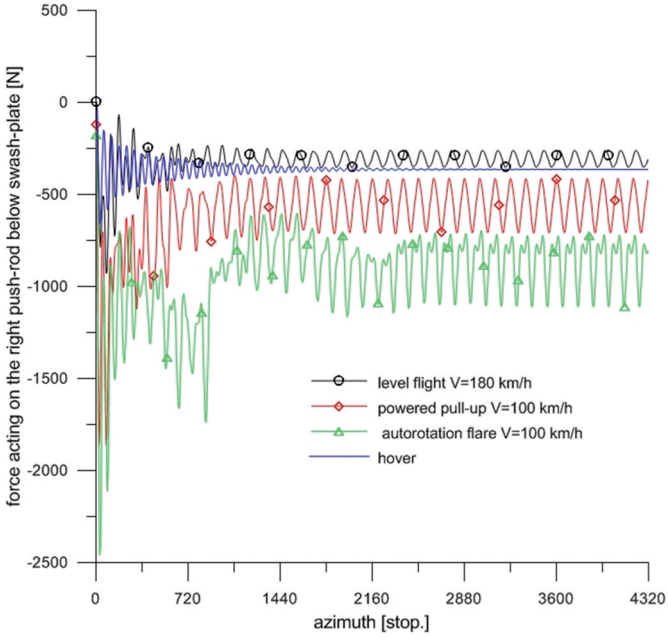

Fig. 14. Comparison of calculated loads of element of rotor control system − force acting on the right push rod below swashplate in certain states of flight ILX-27 helicopter, mass 1,100 kg [J. Stanisławski, 2014]

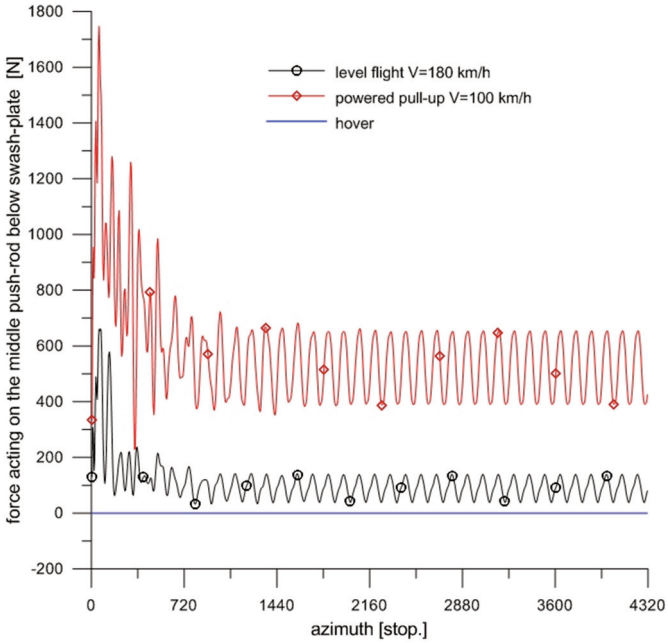

Fig. 15. Comparison of calculated loads of element of rotor control system − force acting on the middle push rod below swashplate in powered states of flight ILX-27 helicopter, mass 1,100 kg, main rotor speed 100% (Ω = 49.65 rd/s) [J. Stanisławski, 2014]

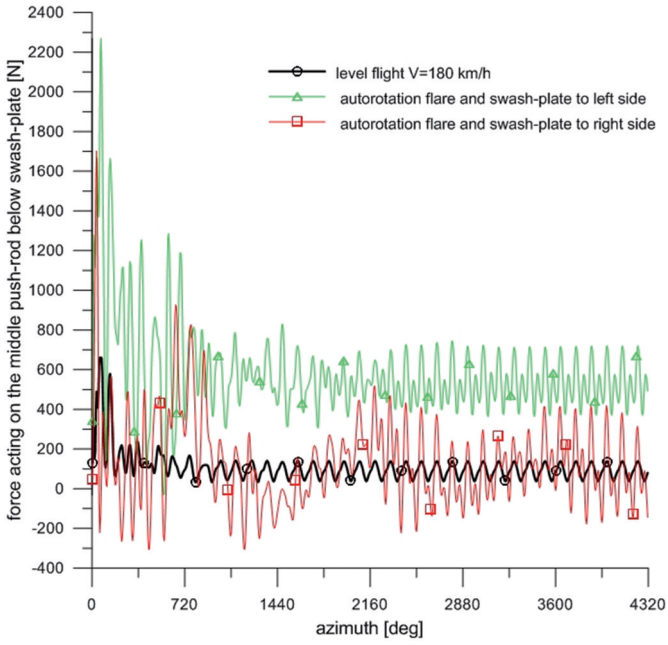

Fig. 16. Comparison of calculated loads of element of rotor control system − force acting on the middle push rod below swashplate in certain states of flight ILX-27 helicopter, mass 1,100 kg, in autorotation rotor speed 122.5% (Ω = 60.8 rd/s) [J. Stanisławski, 2014]

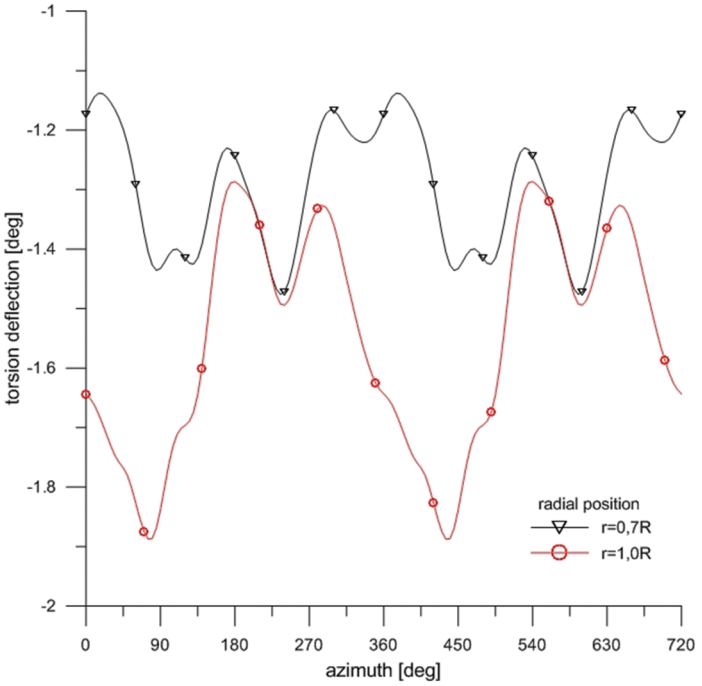

Fig. 17. Changes of blade torsion deflection due to azimuth and radial position of cross-section in flight at high speed [J. Stanisławski, 2014]

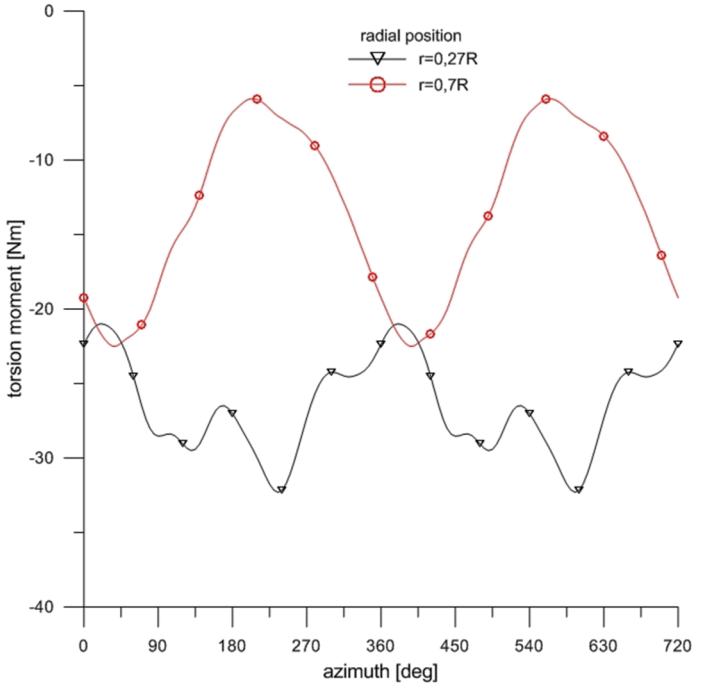

Fig. 18. Changes of blade torsion moment due to azimuth and radial position of cross-section in flight at high speed [J. Stanisławski, 2014]

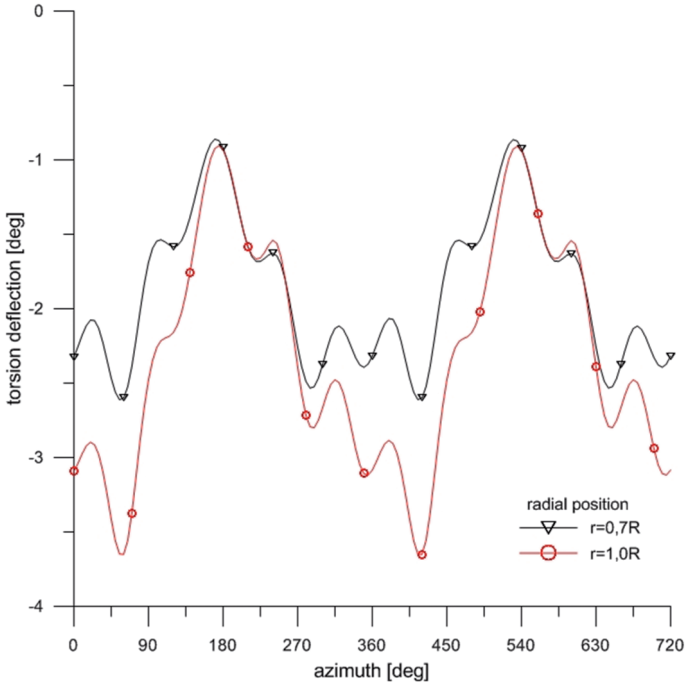

Fig. 19. Changes of blade torsion deflection due to azimuth and radial position of cross-section in flare maneuver [J. Stanisławski, 2014]

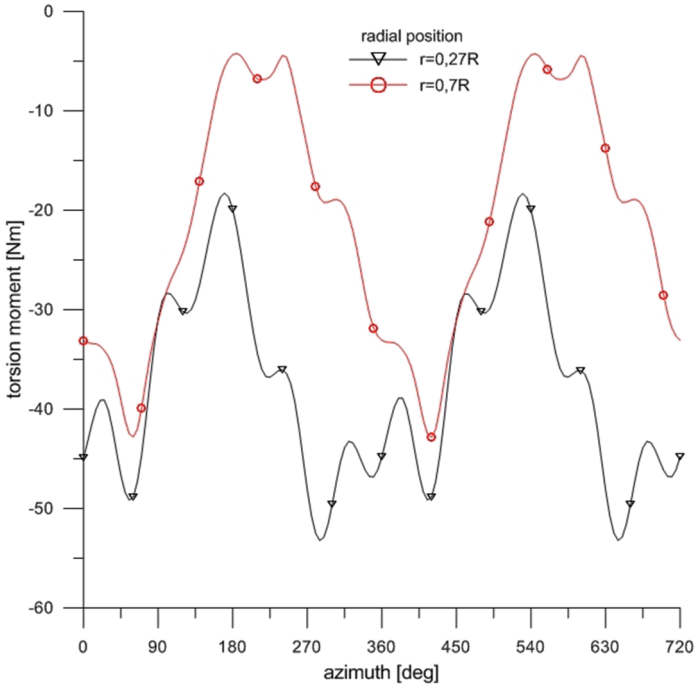

Fig. 20. Changes of blade torsion moment due to azimuth and radial position of cross-section in flare maneuver [J. Stanisławski, 2014]

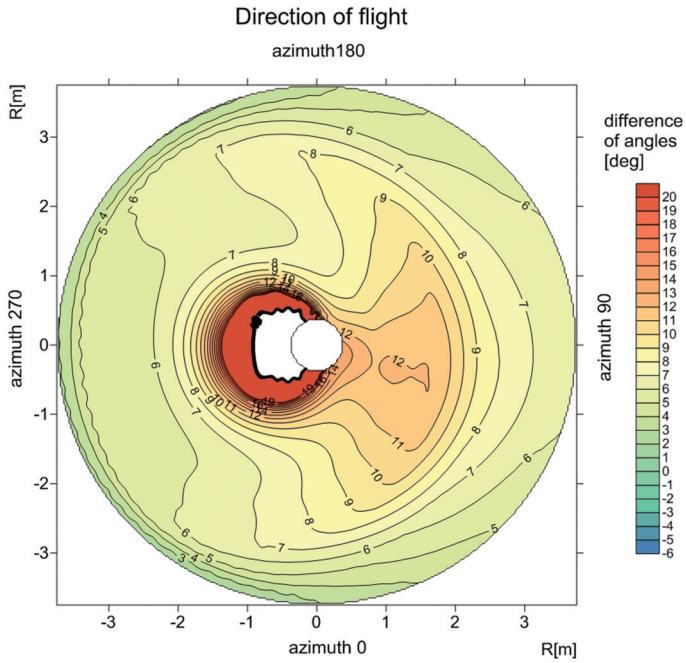

Fig. 21. Rotor disk distribution of difference of critical and local attack angles of blade cross-sections in quasi-static state of flight at high speed [J. Stanisławski, 2014]

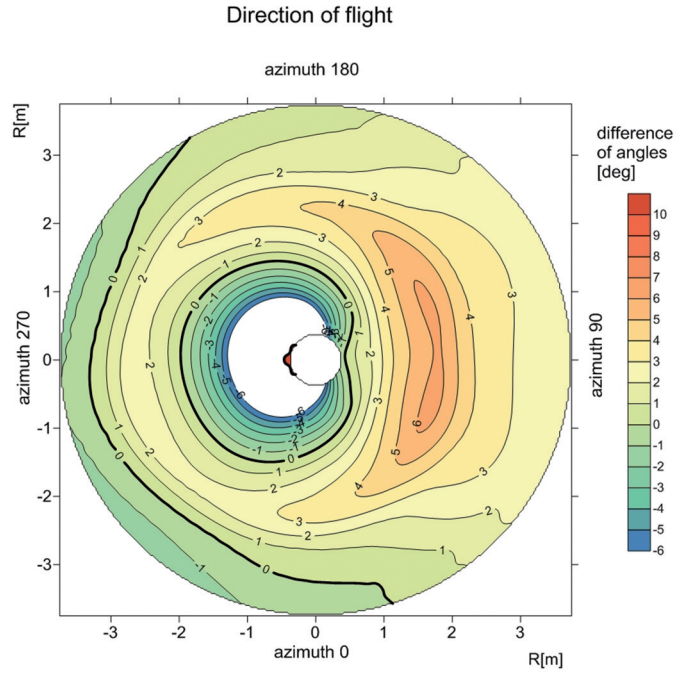

Fig. 22. Rotor disk distribution of difference of critical and local attack angles of blade cross-sections in quasi-static state of pull up maneuver, negative value of difference indicates the zone of airflow separation [J. Stanisławski, 2014]

REFERENCES

[1] Guła, P., Gorecki, T. (2013). Design, experiments and development of a Polish unmanned helicopter ILX-27, 39th European Rotorcraft Forum, Moscow, 3-6 September 2013.
[2] Stanisławski, J. (2012). Obliczenia obciążeń śmigłowca ILX-27, Institute of Aviation, internal report ILX27/0001/BP2/2012, Warszawa, (in Polish).
[3] Stanisławski, J. (2013). Porównanie wyników pomiarów oraz symulacji obliczeniowych pracy śmigłowca ILX-27, Institute of Aviation, internal report ILX27/0014/BP2/2013, Warszawa, (in Polish).

EKSPERYMENTALNE I SYMULACYJNE OKREŚLENIE WIELKOŚCI OBCIĄŻEŃ UKŁADU STEROWANIA WIRNIKIEM ŚMIGŁOWCA

Streszczenie

Przedstawiono porównanie wyników pomiarów z prób w zawisie śmigłowca ILX-27 oraz obliczeń symulacyjnych dotyczących obciążeń układu sterowania wirnikiem nośnym. Do obliczeń użyto program komputerowy do wyznaczania obciążeń wirnika śmigłowca z uwzględnieniem odkształcalności łopat. Obliczeniowo wyznaczono poziom obciążeń układu sterowania wirnikiem w wybranych stanach lotu śmigłowca.

Słowa kluczowe: śmigłowiec, łopata, obciążenia układu sterowania.